Rheological Microscopy: Local Mechanical Properties from Microrheology

D. T. Chen,[1] E. R. Weeks,[2] J. C. Crocker,[3] M. F. Islam,[1] R. Verma,[1] J. Gruber,[1]
A. J. Levine,[4] T. C. Lubensky,[1] and A. G. Yodh[1]

[1]*Department of Physics and Astronomy, University of Pennsylvania, Philadelphia, Pennsylvania 19104*
[2]*Department of Physics, Emory University, Atlanta, Georgia 30322*
[3]*Department of Chemical and Biomolecular Engineering, University of Pennsylvania, Philadelphia, Pennsylvania 19104*
[4]*Department of Physics, University of Massachusetts, Amherst, Amherst, Massachusetts 01003*

(Received 25 September 2002; published 14 March 2003)

We demonstrate how tracer microrheology methods can be extended to study submicron scale variations in the viscoelastic response of soft materials; in particular, a semidilute solution of λ-DNA. The polymer concentration is depleted near the surfaces of the tracer particles, within a distance comparable to the polymer correlation length. The rheology of this microscopic layer alters the tracers' motion and can be precisely quantified using one- and two-point microrheology. Interestingly, we found this mechanically distinct layer to be twice as thick as the layer of depleted concentration, likely due to solvent drainage through the locally perturbed polymer structure.

DOI: 10.1103/PhysRevLett.90.108301 PACS numbers: 82.70.Dd, 05.40.–a, 83.60.Bc, 83.80.Lz

The microscopic propagation of force in mechanically inhomogeneous materials is central to many issues in condensed-matter research, including force chains in granular and jamming materials, dynamical heterogeneity in glassy systems, and the behavior of nanocomposite materials. In a different vein, cell biologists have discovered that many aspects of a cell's gene expression, locomotion, differentiation, and apoptosis are also governed by the stress and elasticity of its surroundings, through a coupling of intracellular stress and biochemical signaling pathways. Experimental methods for directly studying microscopic stress and viscoelasticity, however, have been slow to appear. The past decade has seen the development of microrheology, which uses tracer motion to assess rheology in much smaller samples and over a broader range of frequencies than conventional rheometry. Typically, the frequency-dependent shear modulus, $G^*(\omega)$, of a material is derived by tracking driven [1,2] or thermal [3–6] motions of embedded micron-sized tracers. To date, microrheology has been applied to biopolymer solutions [3–5], concentrated emulsions [3], gels [4], and the cytoskeleton of living cells [1,6].

Tracers naturally probe viscoelasticity on length scales comparable to their size. In materials heterogeneous on those scales, tracer motion depends on both the local and the bulk rheology in a complex way [7]. This fact has largely precluded the use and interpretability of microrheology in mechanically heterogeneous materials where such microscopic information is most needed. In this Letter, we demonstrate an analytical framework to separately determine the local and the bulk mechanical properties from microrheology data; a method we term "rheological microscopy." Elaborations of this approach provide routes to understanding nonuniform force propagation in a variety of heterogeneous media.

We demonstrate rheological microscopy on a model system of polystyrene spheres in an aqueous semidilute solution of nonadsorbing, monodisperse semiflexible polymer, λ-DNA. Previous experiments have characterized this model semidilute polymer solution, determining correlation length and, ergo, the microstructure of the depletion layer surrounding the embedded particles, as a function of polymer concentration [8]. Measurements were performed at a variety of sphere diameters and polymer concentrations, allowing us to vary the bulk solution viscoelasticity and the depletion layer thickness relative to the particle size. Experiments reveal the extent of the rheologically distinct layer, which was approximately 2 times the correlation length in the polymer solution, significantly different from the predictions of mean-field theory. The computed bulk rheology is in excellent agreement with independent measurements made using "two-point" microrheology [7,9,10], a method which uses multiple particle correlations to compute the bulk modulus in heterogeneous media.

Passive, or thermally driven, microrheology uses the generalized Stokes-Einstein relation (GSER),

$$\langle \Delta \tilde{r}^2(s) \rangle = \frac{k_B T}{\pi a s \tilde{G}_1(s)}, \tag{1}$$

to determine the single-particle shear modulus $\tilde{G}_1(s)$ from the measured single-particle mean-square displacement, $\langle \Delta r^2(\tau) \rangle = \mathrm{MSD1}$ [3]. Here $\Delta \tilde{r}^2(s)$ is the Laplace transform of $\Delta r^2(\tau)$ as a function of Laplace frequency s, a is the particle radius, and $k_B T$ is the thermal energy. Equation (1) is the familiar Stokes-Einstein relation generalized to a frequency-dependent viscosity, $s^{-1}\tilde{G}_1(s)$. Shear moduli and MSD1 may be readily converted between the Fourier, Laplace, and lag time domains with simple numerical routines [3]. The GSER accurately provides the complex shear modulus $G^*_{\mathrm{bulk}}(\omega) = G'(\omega) + iG''(\omega)$ when the medium is homogeneous on the scale

of a. When the sample is heterogeneous, this GSER can lead to incorrect shear moduli [7,11].

Two-point microrheology is based on cross correlating the motion of pairs of embedded tracers. We begin by following several dozen tracers' thermal motion using video particle tracking. We can then compute the outer product of two different tracers' vector displacements (separated by R) during a lag time τ. Ensemble- and time-averaging such outer products over all trajectory pairs yields a mobility correlation tensor D_{ij} that reports the degree of correlation between the tracers' random motion during lag time τ as a function of their separation R [9]. The shear modulus may be calculated using the relation:

$$\tilde{D}_{rr}(R, s) = \frac{k_B T}{2\pi R s \tilde{G}_2(s)}, \quad (2)$$

where $\tilde{D}_{rr}(R, s)$ is the Laplace transform of $D_{rr}(R, \tau)$, the tensor component directed along the line connecting the centers of two different tracers. In general, the two-point correlation is due to long-wavelength thermal strain undulations of the medium that move the two probes in phase. Importantly, if the medium is a coarse-grained continuum on the scale R and $R \gg a$, D_{ij} is independent of the probes' boundary conditions and geometry [7,11].

Motivated by the similarity between Eqs. (1) and (2), we define the two-point mean-square displacement as MSD2 $= (2R/a)D_{rr}(R, \tau)$. Mechanical heterogeneity, such as expected from a steric depletion zone surrounding a tracer, leads to differences between MSD1 and MSD2. Levine and Lubensky have computed both the effective one- and two-particle viscoelastic response functions for a simple model—tracers surrounded by shells whose rheological properties differ from the bulk [7].

Our experiments were carried out on solutions of bacteriophage lambda DNA (λ-DNA; New England Biolabs Inc.) whose single-stranded ends were filled in with standard techniques [12], suspended in a 10 mM TE buffer (10 mM tris-HCl, 0.1 mM ethylenediaminetetraacetic acid, pH $= 8.0$). λ-DNA has a persistence length of 50 nm, a contour length of 16.5 μm, and a radius of gyration of $R_g \approx 500$ nm [8]. We worked with four semidilute DNA concentrations (30, 104, 190, and 397 μg/ml). The polymer correlation length has been measured to be 350, 190, 130, and 90 nm, respectively, for those concentrations [8]. The critical overlap concentration c^* is roughly 30 μg/ml [13].

We used fluorescent beads as tracers (Molecular Probes, Rhodamine Red-X labeled carboxylate-modified polystyrene). Beads of three different diameters ($2a = 2.0$, 0.97, and 0.46 μm) were dispersed in the DNA solutions at a volume fraction $\phi \approx 10^{-4}$. D_2O was used for density matching. We imaged the samples with bright field microscopy ($2a = 0.97$ μm) or epifluorescence microscopy ($2a = 0.46$, 2.0 μm), with the temperature controlled to 28 °C. We used a 63× water-immersion objective (NA = 1.2) for the 0.46 and 0.97 μm samples and a 20× (NA = 0.7) multi-immersion objective for the 2.0 μm samples, adjusting the particle volume fraction so there were about 100 tracers in each image. Depletion-induced aggregates were screened automatically by our analysis software. To minimize wall effects, we focused roughly 60 μm into the 120 μm thick sealed sample chambers. We used a video shutter time of 2 msec. One hour of video was recorded for each sample yielding $\sim 10^7$ particle positions with 20 nm spatial and 60 Hz temporal resolution. The images were digitized and analyzed off-line, using methods described elsewhere [14].

In Fig. 1 we exhibit the MSD1 and MSD2 for the three different particles sizes at the highest DNA concentration (397 μg/ml, $c \approx 13c^*$). We have rescaled both sets of curves by $a/2\tau$ to highlight deviations from diffusion (wherein the MSD's $\sim\tau$). At early lag times, subdiffusive behavior ($\sim \tau^\alpha$, $\alpha \leq 1$) of the MSD's reflect an elastic response arising from entanglements in the polymer network. At longer times, the MSD's are diffusive and become horizontal, reflecting the relaxation of entanglement stresses. In the inset in Fig. 1, we show the rescaled MSD1, MSD2 for the buffer-only sample (i.e., $c_{\mathrm{DNA}} = 0$). As expected, the two are equal within signal-to-noise and exhibit a linear dependence with respect to τ.

The two-point data collapse onto a single curve independent of particle size, separated from the one-point data. The collapse enabled us to globally determine a master MSD2 curve for each concentration by averaging the different-particle-size MSD2's. The master curve provides bulk solution properties. The one-point data differ primarily because the particle-to-cavity size ratio differs for the different particle sizes. Agreement between MSD2 and MSD1 is best for the largest particle size

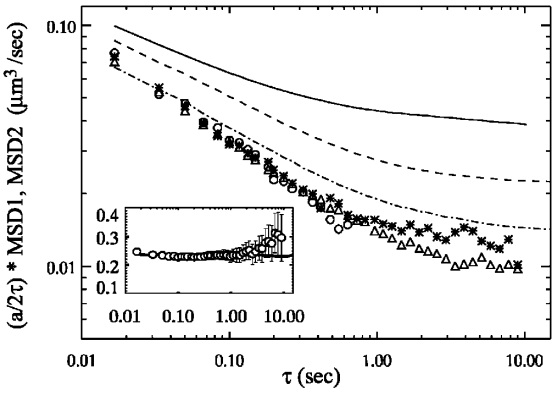

FIG. 1. MSD1 (lines) and MSD2 (symbols) rescaled by $a/2\tau$ for fixed DNA concentration (397 μg/ml, $c \approx 13c^*$) and varying particle size. Solid, dashed, and dot-dashed lines are MSD1 for $2a = 0.46$, 0.97, and 2.0 μm, respectively. Circles, triangles, and stars are MSD2 for $2a = 0.46$, 0.97, and 2.0 μm, respectively. Inset: Rescaled MSD1 (line) and MSD2 (circles) for a Newtonian fluid ($c_{\mathrm{DNA}} = 0$) and particle diameter $2a =$ 2.0 μm.

where the ratio of particle-plus-depletion-layer diameter to particle diameter is closest to unity. The disagreement reflects an effective "slip" between the particles and the bulk solution, due to the depletion cavity.

We determined frequency-dependent complex shear moduli $[G_1^*(\omega), G_2^*(\omega)]$ using the Fourier representation of Eq. (1) along with local algebraic approximations for the MSD's [15,16]. Figure 2(a) shows results for three particle sizes derived from MSD1 and the master MSD2 for a DNA concentration of 397 μg/ml ($c \approx 13c^*$). Figure 2(b) shows moduli for the next lower concentration, 190 μg/ml ($c \approx 6c^*$). In both cases, one-point measurements produce a family of curves displaced from one another and from the two-point results. From this observation, we infer that G_1 underestimates bulk moduli to a greater degree as particle size decreases.

In the inset in Fig. 3(a) the major parameters of the shell model are defined, including the particle-cavity composite radius $b = a + \Delta$, the local cavity shear modulus $G^*_{\rm loc}$, and the bulk shear modulus $G^*_{\rm bulk}$. Using this hydrodynamic model, Levine and Lubensky demonstrated that two-particle correlations for $R \gg a, b$ reflect predominantly bulk responses, whereas the single-particle measurement is sensitive to both bulk and local rheologies. They provide a formula relating the one- to two-particle derived shear moduli $[G_1^*(\omega), G_2^*(\omega)]$. Assuming incompressible media and stick boundary conditions between the solvent and particle,

$$G_2(\omega)/G_1(\omega) = \frac{4\beta^6\kappa'^2 - 9\beta^5\kappa\kappa' + 10\beta^3\kappa\kappa' - 9\beta\kappa'^2 - 15\beta\kappa' + 2\kappa\kappa''}{2[\kappa'' - 2\beta^5\kappa']}. \quad (3)$$

Here $\beta = a/b$, $\kappa = G^*_{\rm bulk}(\omega)/G^*_{\rm loc}(\omega)$, $\kappa' = \kappa - 1$, and $\kappa'' = 3 + 2\kappa$. We use this relation along with our one- and two-point measurements to probe the depletion-induced mechanical heterogeneity.

If the shell model is valid, then we can generate $G_2^*(\omega)$ from the $G_1^*(\omega)$ using Eq. (3). At fixed DNA concentration, the $G_2^*(\omega)$ derived from measurements with different particle diameters will collapse for a specific value of the shell thickness Δ. Our analysis scheme finds an effective layer thickness Δ from this "blind" collapse of the synthetic $G_2^*(\omega)$. We expect Δ to be of order the correlation length ξ based on a simple model of the viscosity dependence with distance from a planar wall for nonadsorbing flexible polymers [7] (see inset in Fig. 4). Moreover, we expect the curves to collapse onto the bulk modulus $G^*_{\rm bulk}(\omega)$, inferred here from the measured $G_2^*(\omega)$. This approach affords a simultaneous determination of the spatial extent of the rheological cavity and the bulk rheological response from one-point data alone.

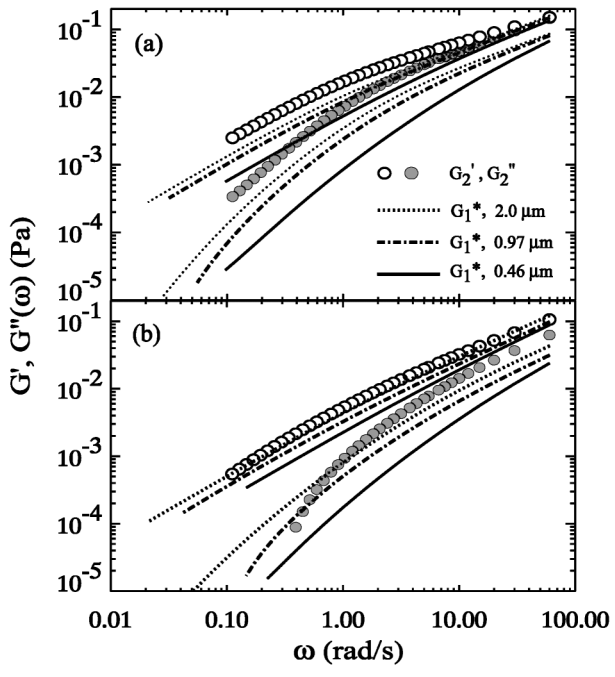

FIG. 2. (a) MSD1- and MSD2-derived bulk shear moduli $G_1^*(\omega), G_2^*(\omega)$ for $c_{\rm DNA} = 397$ μg/ml and different particle sizes. G'' (open circles), G' (solid circles) from master MSD2. Dotted, dash-dotted, and solid lines are G_1^* for $2a =$ 2.0, 0.97, and 0.46 μm particles, respectively. The upper group of lines are G'' while the lower group are G'. (b) $G_1^*(\omega), G_2^*(\omega)$ for $c_{\rm DNA} = 190$ μg/ml.

We determined the collapse of the data for our three particle sizes by treating Δ as a free parameter in the minimization of the standard deviation of the synthetic $G_2^*(\omega)$. We assumed the local modulus is that of a viscous fluid with the viscosity of the solvent, $G_{\rm loc}(\omega) = -i\omega\eta_0$ with $\eta_0 = 0.94$ mPa s. In Fig. 3(a) we exhibit results of the minimization for $c_{\rm DNA} = 397$ μg/ml, where $c \approx 13c^*$. The collapse is nearly perfect with $\Delta =$ 194 nm. As a further check, we applied the method to the next lower concentration $c_{\rm DNA} = 190$ μg/ml, where $c \approx 6c^*$. The results [Fig. 3(b)] again show a good collapse of all particle sizes and the two-point data. The fact that the synthetic G_2 agree with the two-point derived $G^*_{\rm bulk}(\omega)$ verifies the applicability of the shell model for a polymer network with depletion-induced inhomogeneities.

Last, we relate the Δ's to our previously measured ξ. In Fig. 4 we plot Δ vs ξ. Our values for Δ are closer to 2ξ (dotted line in Fig. 4), suggesting that the "rheological" cavity size for the depleted particles are of order ξ, albeit a bit larger. A naive mean-field treatment (see the width at half maximum of the local viscosity in the inset in Fig. 4) leads to $\Delta = 1.33\xi$, which is drawn with the dash-dotted line. Our values for Δ are closer to 2ξ as shown with the

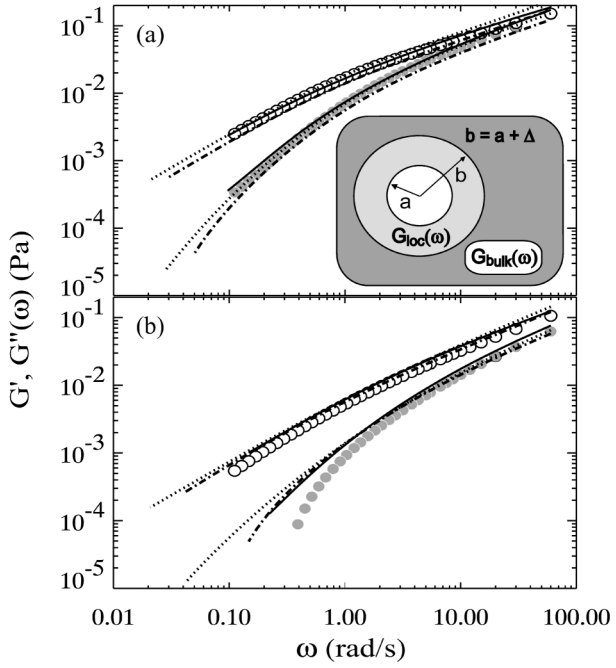

FIG. 3. (a) $G_2^*(\omega)$ obtained from shell model using the collapse of the G_1 data for $c_{\mathrm{DNA}} = 397\ \mu$g/ml. Circles are the measured G', G'' (open, solid). Lines are different particle diameters 2.0, 0.97, and 0.46 μm (dotted, dash-dotted, and solid). Lines resulted from using an effective shell thickness $\Delta = 194$ nm and solvent viscosity $\eta = 0.94$ mPa s. The lines agree with the measured bulk moduli from two-point $G_2^*(\omega)$ (open, solid circles). Inset: shell model of Levine and Lubensky [7]. (b) Results for $c_{\mathrm{DNA}} = 190\ \mu$g/ml obtained with $\Delta = 336$ nm.

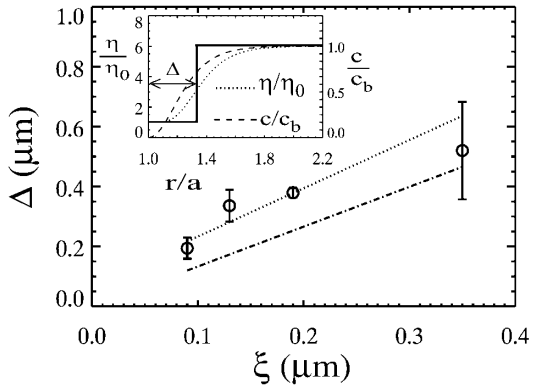

FIG. 4. Effective layer thickness Δ determined from optimal collapse of the G_1 data for all particle sizes vs measured correlation length ξ. Dash-dotted line: $\Delta = 1.33\xi$. Dotted line: $\Delta = 2\xi$. Inset: variation of solution viscosity (dotted line) and DNA concentration (dashed line) with dimensionless distance from the sphere for $c = 190\ \mu$g/ml, $2a = 0.97\ \mu$m. The width at half maximum of the viscosity profile is used to define an effective cavity thickness Δ for the shell model (solid line).

dotted line. The underestimate by mean-field theory could arise from hydrodynamic penetration of the solvent flow into the outer edges of the shell, an effect which is not captured in the mean-field treatment.

To conclude, we have used one- and two-point microrheological measurements and theory to determine the rheological microstructure of depletion-induced layers surrounding a tracer particle in a semidilute polymer solution. Furthermore, we have shown how the collapse of conventional one-point microrheological measurements can be applied to extract bulk viscoelastic moduli, a quantity heretofore unambiguously accessible only to two-point measurements of such systems. Equivalently, if one has knowledge of cavity size, the rheology of the layers can be deduced. Refinements, both theoretical and experimental, of the basic rheological microscopy method we have presented here should enable its extension to the study of more complex media.

We thank A. W. C. Lau and B. D. Hoffman for helpful discussions. We gratefully acknowledge support from the NSF (DMR-0203378), PENN MRSEC (DMR-0079909), and NASA (NAG8-2172).

[1] B. Fabry *et al.*, Phys. Rev. Lett. **87**, 148102 (2001).
[2] L. A. Hough and H. D. Ou-Yang, J. Nanopart. Res. **1**, 495 (1999).
[3] T. G. Mason and D. A. Weitz, Phys. Rev. Lett. **74**, 1250 (1995).
[4] B. Schnurr *et al.*, Macromolecules **30**, 7781 (1997); F. Gittes *et al.*, Phys. Rev. Lett. **79**, 3286 (1997).
[5] T. G. Mason *et al.*, Phys. Rev. Lett. **79**, 3282 (1997).
[6] S. Yamada, D. Wirtz, and S. C. Kuo, Biophys. J. **78**, 1736 (2000)
[7] A. J. Levine and T. C. Lubensky, Phys. Rev. E **65**, 011501 (2001). We calculated the variation of viscosity from the surface of the particle following the derivation given in Appendix B. However, we assumed $\xi \sim \phi^{-1/2}$ consistent with our findings in [8]. The resulting expression, $\eta = \eta_0 + \eta_p \tanh^5(x/\xi)$, was used to estimate the effective width Δ of the depletion layer.
[8] R. Verma *et al.*, Macromolecules **33**, 177 (2000); R. Verma *et al.*, Phys. Rev. Lett. **81**, 4004 (1998).
[9] J. C. Crocker *et al.*, Phys. Rev. Lett. **85**, 888 (2000).
[10] L. Starrs and P. Bartlett, Faraday Discuss. **123**, 323 (2003). Their experiment was similar in spirit to ours, but they attributed observed differences in one- and two-particle measurements to variations in the stick-slip boundary condition of the particles with respect to the polymeric solution.
[11] A. J. Levine and T. C. Lubensky, Phys. Rev. Lett. **85**, 1774 (2000).
[12] J. Sambrook, E. F. Fritsch, and T. Maniatis, in *Molecular Cloning–A Lab Manual* (Cold Spring Harbor Laboratory Press, New York, 1989), 2nd ed.
[13] N. Pernodet and B. Tinland, Biopolymers **42**, 471 (1997).
[14] J. C. Crocker and D. G. Grier, J. Colloid Interface Sci. **179**, 298 (1996).
[15] B. R. Dasgupta *et al.*, Phys. Rev. E **65**, 051505 (2000).
[16] T. G. Mason, Rheol. Acta **39**, 371 (2000).